

## ANALYZING SELF-IGNITION IN RAPIDLY COMPRESSED TURBULENCE

**Guillaume Lodier**

CORIA - CNRS and INSA de Rouen  
76801 Saint-Etienne-du-Rouvray, France  
email: guillaume.lodier@laposte.net

**Pascale Domingo**

CORIA - CNRS and INSA de Rouen  
76801 Saint-Etienne-du-Rouvray, France  
email: domingo@coria.fr

**Luc Vervisch**

CORIA - CNRS and INSA de Rouen  
76801 Saint-Etienne-du-Rouvray, France  
email: vervisch@coria.fr

### ABSTRACT

A method to estimate the propagation speed of an ignition front in Direct Numerical Simulation (DNS) is discussed. It is based on the time evolution of perfectly stirred reactors starting at various fresh-gas ignition temperatures. The proposed approach is applied to DNS of a rapid compression machine, in which the mixture composition is homogeneous, but the temperature distribution is non-uniform due to heat-transfer at wall. The two expected distinct ignition regimes are reported, one where combustion propagates at the speed of sound or even above and occurring over a large portion of the combustion chamber, with a strong and sudden pressure increase; another one, much more localized in space and with a flame propagation pertaining to a deflagration mode.

### INTRODUCTION

The physics of ignition of a mixture homogeneous in concentration has been the subject of multiple studies (Zel'dovich, 1980; Bartenev & Gelfand, 2000; Sreedhara & Lakshminisha, 2002; Dec, 2009; Gu *et al.*, 2003; Mastorakos, 2009; Kalghatgi *et al.*, 2011). Among the numerous results reported in the case of a rapid compression two main ignition scenarios were discussed, delineating between homogeneous and fragmented ignition regimes. With actual DNS tools, this point was recently revisited trying to elucidate the origin of these two specific regimes (Lodier *et al.*, 2012).

Direct Numerical Simulation of an experimental setup (Guibert *et al.*, 2010, 2007), in which a reactive mixture is rapidly compressed in a combustion chamber after passing through turbulence-grid, has been performed with a fully compressible flow solver, using a structured mesh with immersed boundaries for the cylindrical wall (Merlin *et al.*, 2013). After comparing with experiments the major flow properties in Large Eddy Simulation, the chamber volume was downsized for Direct Numerical Simulation with single-step chemistry, using about 70 million nodes and a resolution of 20  $\mu\text{m}$ , but preserving the flow admission sequence properties. All the details concerning the simulation procedure may be found in Lodier *et al.* (2012).

Heat transfer at wall of the cylinder rapidly promotes a weakly stratified temperature field and mechanisms controlling the birth of ignition under these conditions may be analyzed. After the rapid compression, coherent flow structures are generated during the admission of the fuel-lean charge in the combustion chamber. The temperature distribution inside these structures evolves according to three phenomena: adiabatic compression, engulfment, and, mixing with colder fluid from wall boundary layers. Accordingly, a competition develops between the adiabatic compression, which increases the temperature of the gaseous mixture, and, mixing with colder fluid from wall, which locally decreases fluid internal energy. Under these conditions, two major ignition scenarios have been recovered:

- For an ignition delay smaller than the time required for turbulent mixing to damp high temperature fluctuations between wall layers and the inside of coherent flow structures, the core of large-scale vortices is almost 'thermally insulated' and ignition will primarily appear inside these flow rollers, which are homogeneously distributed over the flow domain, leading to a global ignition phenomena.
- When turbulent mixing has sufficiently influenced the flow before ignition so that the temperature fluctuations are distributed all over the combustion chamber, the starting of ignition will be controlled by very localized details of the flow topology, as for instance local compression zones between coherent structures, where the flow divergence is an additional source of temperature, favoring the starting of combustion. Ignition is then found to be non-global, but rather scattered.

The present paper is in the continuation of this work, focussing on a novel method to determine the gradient of ignition delay, and thus the propagation speed of the ignition front, at a given instant in time in a three-dimensional simulation. From the results, it is shown that strong pressure waves are likely to appear in the case of ignition within large-scale coherent structures.

Ignition	$T_{Ac}/T_o$	$\tau_{ig}/t_{TDC}$	$u'/U_o(t)$
Case (1)	48	0.976	10%
Homogeneous			
Case (2)	52	1.134	10%
Fragmented			

Table 1. Cases simulated.  $T_{Ac}$ : activation temperature,  $T_o = 343$  K.  $\tau_{ig}$ : ignition delay.  $t_{TDC} = 29$  ms.  $u'/U_o(t)$ : turbulence intensity at admission,  $U_o(t)$  bulk velocity in admission plane (Lodier *et al.*, 2012).

## Flow configuration

The geometry studied refers to the Rapid Compression Machine reported in Guibert *et al.* (2010). This machine, sketched in Fig. 1(a), is mainly composed of an hydraulic system, a piston moving inside a pre-compression volume and the combustion chamber. Initially, at  $t = 0$ , the mixture to be analyzed is contained within a volume decomposed into the pre-compression chamber, a convergent section, the piston nose lodging section and the combustion chamber. The pre-combustion chamber is a 200 mm long stainless steel tube of 91.5 mm diameter through which the piston moves to rapidly compress the mixture. The convergent section is 50 mm long and connect the 91.5 mm diameter tube with the 40 mm diameter combustion chamber, that is 44 mm long. The end of the convergent section stops the piston, the whole volume of gas is thus compressed into the combustion chamber, with a known dead-flow volume trapped between the piston and the convergent (i.e. this volume  $V^*$  of gas does not enter the combustion chamber). The combustion chamber is made of quartz, to provide optical access, and a turbulence grid is placed at its inlet. A complete description of the experimental device is found in Guibert *et al.* (2007).

The duration of admission is  $t_{TDC} = 29$  ms, where 'TDC' denotes the top-dead-center (i.e. the piston reaches its final position and stops). In the simulation, this compression is controlled by the time distribution of bulk velocity during injection, which allows for reproducing the experimental pressure signal. The exact piston speed is used to define the admission velocity of the combustion chamber from mass conservation, accounting for various flow volumes through geometrical parameters (Lodier *et al.*, 2012). The chemical source is expressed in the simulation with a single-step Arrhenius chemistry, using two sets of parameters leading to ignition right before or after  $t = t_{TDC}$ ; these parameters and their corresponding ignition regimes are given in Table 1.

The properties of the very early development of ignition in a homogeneous fuel/air mixture (uniform equivalence ratio) is controlled by the temperature distribution, which is a marker of the internal energy available in the flow to trigger combustion. Figure 2 shows iso-contour of Q-criterion colored by temperature. The temperature evolution results from both the adiabatic compression (increase of temperature) and heat-transfer at wall (decrease of temperature), leading to temperature fluctuations of the order of 30 K.

In the DNS, the temperature is obtained from the solving of a balance equation for the total energy. However, to

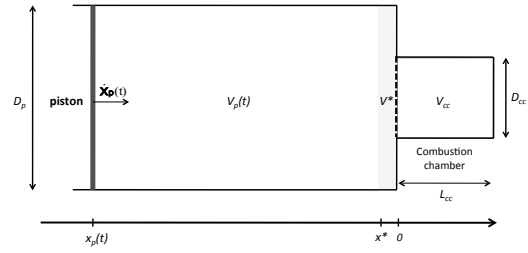


Figure 1. Sketch of the Rapid Compression Machine (Guibert *et al.*, 2010).  $D_{cc}$ ,  $V_{cc}$ : Diameter and volume of the combustion chamber.  $V^*$ : dead-flow volume.  $D_p$ : piston diameter.  $x_p(t)$ : piston position.  $V_p(t)$ : Volume to be swept by the piston.  $x^* = x_p(t = t_{TDC})$ : top-dead-center position.

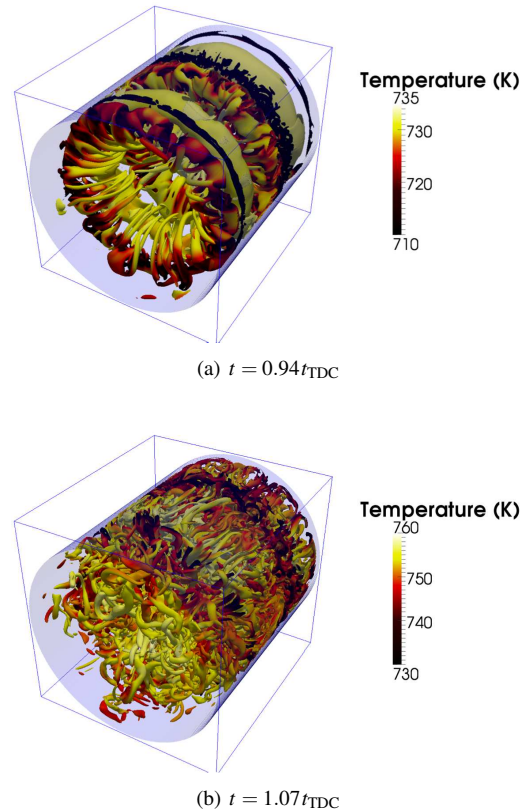


Figure 2. Iso-contour of Q-criterion ( $Q = 15 \cdot 10^6 \text{ s}^{-2}$ ) colored by temperature. Flow goes from left to right.

isolate the various effects contributing to the temperature evolution, a specific balance equation may be written, neglecting viscous heating and with usual notations:

$$\rho C_p \frac{DT}{Dt} = \nabla \cdot (\lambda \nabla T) + \rho \dot{\omega}_T + \frac{DP}{Dt}, \quad (1)$$

or again using the continuity equation and the perfect gas law  $P = \rho rT$ , with constant heat capacities:

$$\rho C_v \frac{DT}{Dt} = \nabla \cdot (\lambda \nabla T) + \rho \dot{\omega}_T - (\gamma - 1) \rho C_v T \nabla \cdot \mathbf{u}. \quad (2)$$

Before combustion occurs, the chemical source of temperature  $\dot{\omega}_T = 0$ . In Lodier *et al.* (2012), it was discussed how  $\nabla \cdot \mathbf{u}$  contributes to both the global adiabatic compression and to very localized temperature variations between vortical structures, which may be sufficient to promote a fragmented ignition regime when all the flow points are actually close to ignition because of the rapid compression.

A progress of reaction  $c$  is defined from the fuel mass fraction (notice that in the DNS  $c$  is not exactly linearly related to temperature because the flow equations are solved in their fully compressible form).  $c = 0$  in fresh gases and  $c = 1$  in fully burnt products.  $\dot{\omega}_T = \Delta h^o \dot{\omega}_c$ , the temperature source is expressed from the progress variable source  $\dot{\omega}_c$ , through  $\Delta h^o$  the heat release by the reaction.

To further analyze the behavior of the ignition spots and their propagation, an analogy is made with isolated perfectly stirred reactors (Colin *et al.*, 2005; Etheridge *et al.*, 2011); a canonical problem that is widely used in the literature to model ignition by rapid compression. Specifically, a method is now discussed to easily extract ignition delay in a 3D flow from these reactors, which are parameterized by their initial temperature  $T_0$ , also called fresh gas temperature. Every reactor evolves over  $t$ , the time, and any quantity may be expressed as:  $\phi = \phi(T_0, t)$ . In particular,  $c = c(T_0, t)$ , in single-step chemistry  $c$  is continuously growing with time and  $t = t^R(T_0, c)$  may be obtained, leading to  $\phi = \phi(T_0, c)$ . Therefore when  $T_0$  and  $c$  are known, the chemical state of the reactor is also fully known.

## Reference fresh gas temperature

In the canonical case of a constant pressure and homogeneous mixture,

$$\rho \frac{dc}{dt} = \rho \dot{\omega}_c, \quad (3)$$

Eq. (1) becomes:

$$\rho C_p \frac{dT}{dt} = \rho C_p \frac{dT}{dc} \dot{\omega}_c = \rho \dot{\omega}_T = \Delta h_c^o \rho \dot{\omega}_c. \quad (4)$$

Similarly, Eq. (2) reads in the homogeneous and constant volume case:

$$\rho C_v \frac{dT}{dc} \dot{\omega}_c = \Delta h_c^o \rho \dot{\omega}_c, \quad (5)$$

With constant heat capacities, integrating the relations (4) and (5) between  $T_0 = T(c=0)$  and  $T = T(c)$  leads to:

$$\text{Constant pressure: } T_0 = T - \frac{\Delta h_c^o}{C_p} c, \quad (6)$$

$$\text{Constant volume: } T_0 = T - \frac{\Delta h_c^o}{C_v} c. \quad (7)$$

From these quantities and from the values of  $T(\underline{x}, t)$  and  $c(\underline{x}, t)$  in the DNS, a three-dimensional field  $T_0(\underline{x}, t)$  of reference fresh gas temperature may be obtained. Then, any quantity  $\phi(T_0(\underline{x}, t), c(\underline{x}, t))$ , tabulated from reactors, may be compared against  $\phi(\underline{x}, t)$ , its DNS value. In the case of constant heat capacities and one-step chemistry, the heat source evolution and any other quantity, behave similarly in constant pressure or constant volume evolutions *vs*  $T$  and  $c$ , as soon as  $T_0$  is calculated according to relations (6) or (7), depending on the chosen type of reactor evolution.

Indeed, it is seen in Fig. 3 that  $\dot{\omega}_c$ , the source of progress variable, is perfectly reproduced by the tabulation if the local value of  $T_0 = T_0(T(\underline{x}, t), c(\underline{x}, t))$  and  $c(\underline{x}, t)$  are taken to enter the reactor lookup table (black dots in Fig. 3). To illustrate the strong impact of temperature fluctuations, the same is done with the overall mean temperature  $\langle T_0 \rangle$ , which is close to the adiabatic compression temperature, then a strong departure between the tabulated response and the DNS one is observed (grey dots in Fig. 3); confirming the importance of accounting for non-homogeneities in temperature within the rapid compression machine. Similar results are found in case (2), not shown for brevity.

These observations suggest that a perfectly stirred reactor, once properly calibrated by  $T_0(\underline{x}, t)$  and  $c(\underline{x}, t)$ , can be used as a sub-model for quantifying every instant in time of the DNS. Notice, however, that because of temperature heterogeneities, every single point of the three-dimensional DNS goes with a given  $T_0$  that is linked to the local temperature  $T$  (relations (6) or (7)),  $T$  which in counterpart depends on the full three-dimensional transport of energy within the flow.

## Determination of the distribution of ignition delay

The three-dimensional distribution of the ignition time-delay,  $\tau_{ig}(\underline{x}, t)$  is an essential ingredient in the analysis of ignition regimes. At every instant in time,

$$u_{sp}(\underline{x}, t) = |\nabla \tau_{ig}(\underline{x}, t)|^{-1} \quad (8)$$

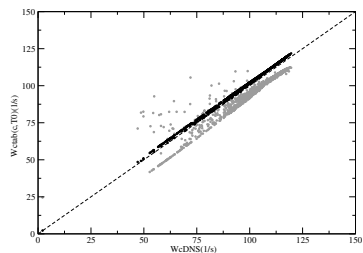
defines the speed of propagation of a potential ignition front. For a spatially uniform  $\tau_{ig}$  distribution, ignition occurs homogeneously; for large gradients of  $\tau_{ig}$ , the propagation of an ignition front may be observed. If the  $\tau_{ig}$  distribution is such that  $u_{sp}$  approaches the speed of sound, a detonation wave may develop (Zeldovich, 1980).

Measuring  $\tau_{ig}$  in experiments or in DNS is far from being obvious, as it depends on the very local flow properties evolving in time. In the perfectly stirred reactor model, for a given fresh gas temperature  $T_0$ , it can be defined as the position in time where the burning rate reaches its maximum, then  $\tau_{ig}^R(T_0)$  is known as a function of  $T_0$  (Fig. 4).

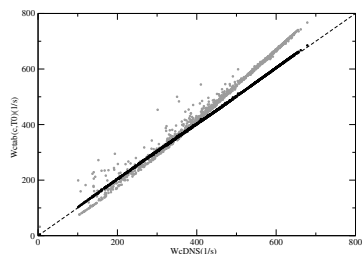
As discussed above,  $t = t^R(T_0, c)$ , the time elapsed in the reactor when a given  $c$ -level of reaction progress is reached, is also known for every fresh-gas temperature  $T_0$ . This information is easily tabulated to determine at any point  $\underline{x}$  of the DNS, the time left before ignition to occur, as the time needed in a reactor to reach ignition starting from  $T_0(\underline{x}, t)$ , minus the time already elapsed in the reactor to reach the progress of reaction  $c(\underline{x}, t)$ :

$$\tau_{ig}(\underline{x}, t) = \tau_{ig}^R(T_0(\underline{x}, t)) - t^R(T_0(\underline{x}, t), c(\underline{x}, t)) \quad (9)$$

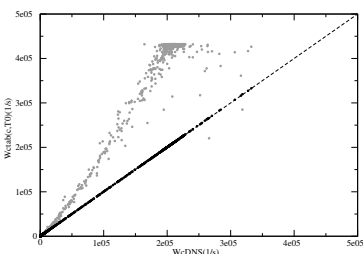
August 28



(a)  $t = 0.983 t_{TDC}$



(b)  $t = 0.983 t_{TDC}$



(c)  $t = 0.987 t_{TDC}$

Figure 3. Scatter plot of  $\hat{\omega}_c(T_0, c)$  vs  $\hat{\omega}_c$  from DNS. Black:  $T_0$  local value from Eq. (7); Grey  $\langle T_0 \rangle$ , Case (1).

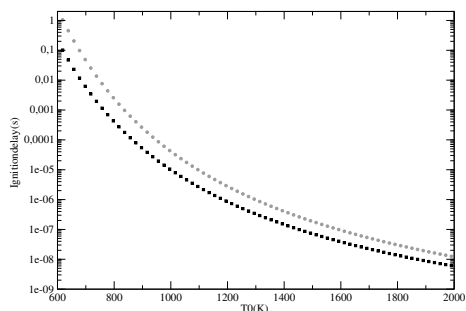
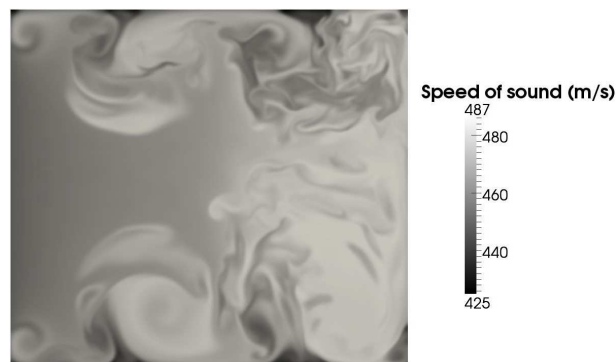


Figure 4.  $\tau_{ig}^R$  vs  $T_0$ , constant pressure evolution. Black: case (1); Grey: case (2) of Table 1.

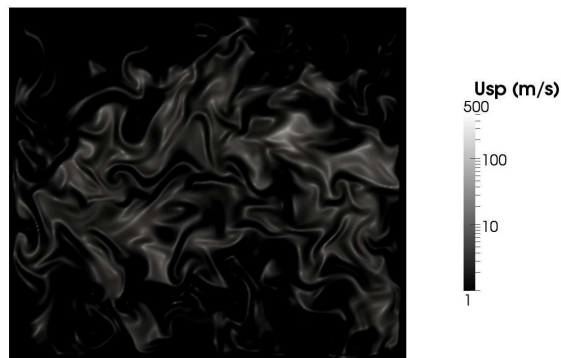
This last relation allows for building and analyzing three dimensional distributions of ignition delay from a DNS field. If the constant pressure relation (6) is used to find  $T_0$  from the DNS temperature  $T$ , then  $\tau_{ig}$  must be taken in the constant pressure reactor, otherwise it is the constant volume relation (7) that must be chosen. As for the progress variable source, the constant volume or constant pressure evolutions will return the same ignition delay vs  $T$ , as soon as the proper relation ((6) or (7)) between  $T$  and  $T_0$  is used.



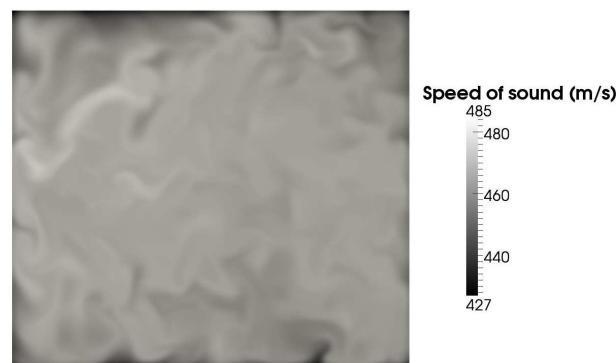
(a) Case (1)  $u_{sp}$  (log scale)



(b) Case (1)  $a$



(c) Case (2)  $u_{sp}$  (log scale)



(d) Case (2)  $a$

Figure 5. Centerline plane of  $u_{sp}$  and of  $a$ , the speed of sound. Case (1) at  $t = 0.983 t_{TDC}$  and Case (2) at  $t = 1.355 t_{TDC}$

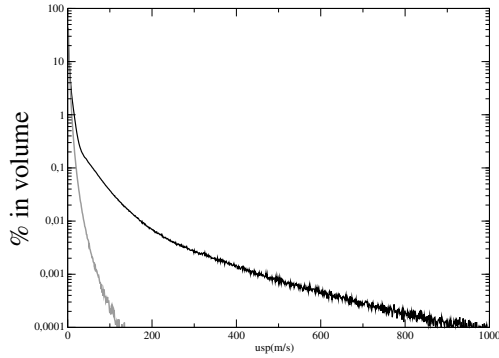


Figure 6. Histogram in % of  $u_{sp}$  (m/s) right before ignition. Black: Case (1) at  $t = 0.983 t_{TDC}$ . Grey: Case (2) at  $t = 1.355 t_{TDC}$ .

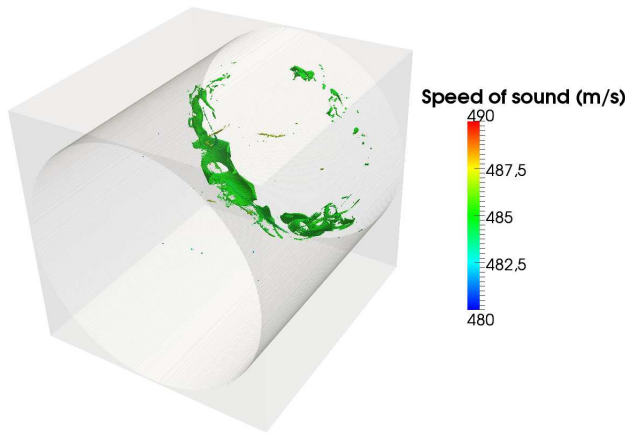


Figure 7. Case (1) at  $t = 0.983 t_{TDC}$ . Iso-surface  $u_{sp} = 485$  m/s colored par the speed of sound.

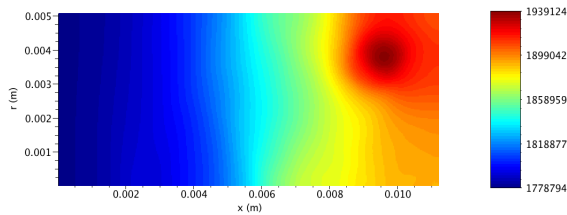


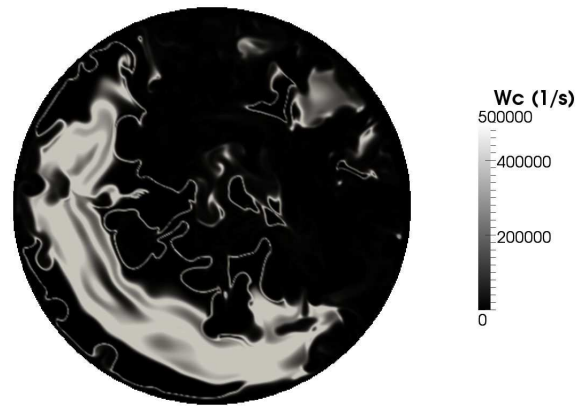
Figure 8. Distribution of radially averaged pressure. Case (1) at  $t = 0.987 t_{TDC}$ .

### Ignition regimes analysis

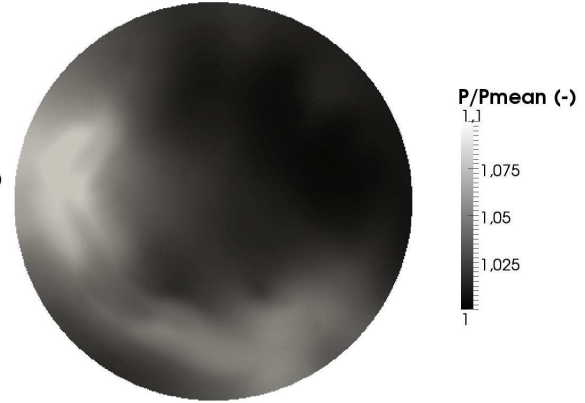
The relation (8) is now combined with Eq. (9) to examine the propagation mode of ignition in both cases (1) and (2) of Table 1, featuring quasi-homogeneous and fragmented ignition, respectively.

The propagation speed of the ignition front  $u_{sp}$  (Eq. (8)) is shown with the speed of sound  $a = \sqrt{\gamma r T}$  in Fig. 5, right before ignition.

- In case (1), in the bottom right corner of Figs. 5(a)-5(b),  $u_{sp} \approx a$ , then a strong and rapid ignition is observed, supporting the previously discussed quasi-



(a) Case (1)  $\dot{\omega}_c$



(b) Case (1)  $P/\langle P \rangle$

Figure 9. Spanwise view of the burning rate and pressure normalized by its mean value. Case (1)  $x = 0.95$  cm and  $t = 0.987 t_{TDC}$ .

homogeneous ignition (Lodier *et al.*, 2012).

- In case (2) (Figs. 5(c)-5(d)),  $u_{sp}$  is always much smaller than the speed of sound, a much smoother ignition process is then reported. This is confirmed in Fig. 6, where it is seen that  $u_{sp}$  features much smaller values in case (2) than in case (1).

The matching between the speed of the ignition front and the speed of sound observed in case (1), is also visible in Fig. (7), where one iso-value of  $u_{sp}$  is colored by the speed of sound, the flow zone concerned here is mainly located within large scale vortices. A fact that is illustrated in Fig. 8, where the pressure distribution has been radially averaged, it is seen that the sudden pressure increase is indeed located within a coherent flow structure.

The two different ignition regimes may be seen in Figs. 9 and 10, quasi-homogeneous in case (1) and localized in case (2). The burning rate  $\dot{\omega}_c$  (Figs. 9(a) and 10(a)) and the pressure (Figs. 9(b) and 10(b)), normalized by its mean value in the combustion chamber (the adiabatic compression pressure level), are shown.

- In the quasi-homogeneous case (1), the pressure field increases by about 10% (Figs. 9(a)-9(b), south-west quadrant). At the same time, a deflagration wave with thin reaction zones and with almost no significant pressure variation is observed in the north-east quadrant. Suggesting that even when one type of ignition regime dominates, other ignition modes may occur simultane-

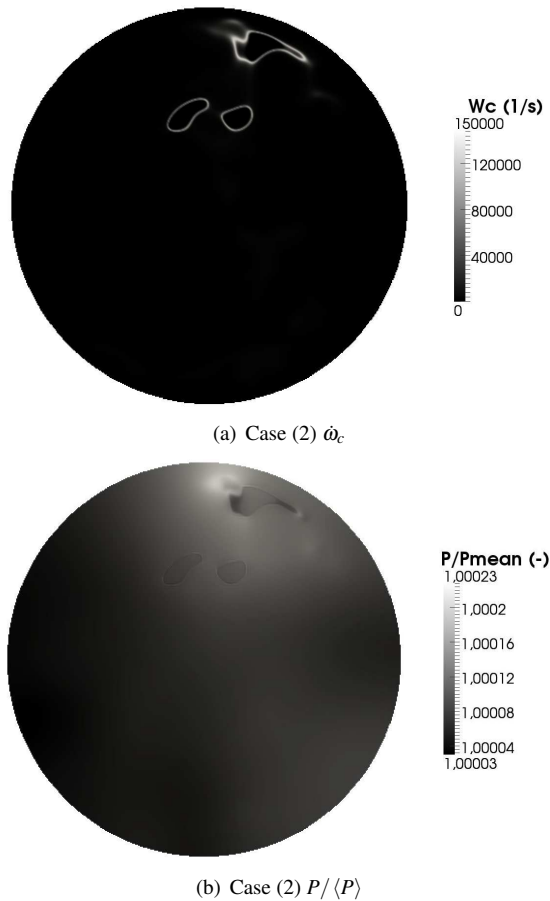


Figure 10. Same as Fig. 9. Case (2)  $x = 0.15$  cm and  $t = 1.375t_{TDC}$ .

ously.

- In the case (2), Figs. 10(a)-10(b), ignition is characterized by a weak pressure jump, representative of the subsonic thermal expansion of the ignition kernel.

## SUMMARY

A novel approach to estimate the propagation speed of ignition fronts in Direct Numerical Simulation has been reported. It is based on the coupling of three-dimensional DNS fields with well-stirred reactor responses.

The proposed methodology is tested in DNS of a rapid compression machine and the two expected ignition regimes, in volume with the possibility of a sonic displacement of the ignition wave, or fragmented with much lower propagation speed of ignition, are recovered with or without

strong pressure waves.

## REFERENCES

- Bartenev, A. M. & Gelfand, B. E. 2000 Spontaneous initiation of detonations. *Progress in Energy and Combust. Sci.* **26** (1).
- Colin, O., Pires da Cruz, A. & Jay, S. 2005 Detailed chemistry-based auto-ignition model including low temperature phenomena applied to 3-d engine calculations. *Proceedings of the Combustion Institute* **30** (2), 2649–2656.
- Dec, J. 2009 Advanced compression-ignition engines - understanding the in-cylinder processes. *Proc. Combust. Inst.* **32** (2), 2727–2742.
- Etheridge, J., Mosbach, S., Kraft, M., Wu, H. & Collings, N. 2011 Modelling cycle to cycle variations in an si engine with detailed chemical kinetics. *Combust. Flame* **158** (1), 179–188.
- Gu, XJ, Emerson, DR & Bradley, D. 2003 Modes of reaction front propagation from hot spots. *Combustion and flame* **133** (1-2), 63–74.
- Guibert, P., Keromnes, A. & Legros, G. 2007 Development of a Turbulence Controlled Rapid Compression Machine for HCCI Combustion. *SAE Technical Paper* **2007-01-1869**.
- Guibert, P., Keromnes, A. & Legros, G. 2010 An Experimental Investigation of the Turbulence Effect on the Combustion Propagation in a Rapid Compression Machine. *Flow, turbulence and combustion* **84** (1), 79–95.
- Kalghatgi, G. T., Hildingsson, L., Harrison, A. J. & Johansson, B. 2011 Autoignition quality of gasoline fuels in partially premixed combustion in diesel engines. *Proc. Combust. Inst.* **33** (1), 3015–3021.
- Lodier, G., Merlin, C., Domingo, P., Vervisch, L. & Ravet, F. 2012 Self-ignition scenarios after rapid compression of a turbulent mixture weakly-stratified in temperature. *Combust. Flame* **159** (11), 3358–3371.
- Mastorakos, E. 2009 Ignition of turbulent non-premixed flames. *Progress in Energy and Combust. Sci.* **35** (1), 57–97.
- Merlin, C., Domingo, P. & Vervisch, L. 2013 Immersed boundaries in large eddy simulation of compressible flows. *Flow Turbulence and Combust.*, Submitted **90** (1), 29–68.
- Sreedhara, S. & Lakshmisha, KN 2002 Autoignition in a non-premixed medium: Dns studies on the effects of three-dimensional turbulence. *Proceedings of the Combustion Institute* **29** (2), 2051–2059.
- Zeldovich, Y.B. 1980 Regime classification of an exothermic reaction with nonuniform initial conditions. *Combustion and Flame* **39** (2), 211–214.